NON-ENZYMATIC DETECTION OF GLUCOSE AND KETONES IN URINE USING PAPER-BASED ANALYTICAL DEVICES

Kamila Rohadatul 'Aisy, Ahmad Luthfi Fahmi, Hermin Sulistyarti, Ika Oktavia Wulandari, Akhmad Sabarudin

Department of Chemistry, Faculty of Science, Brawijaya University, Malang, Indonesian

ARTICLE INFO	ABSTRACT
  	Diabetes, driven by unbalanced diets and unhealthy lifestyles, is highly prevalent. In Indonesia, its prevalence is projected to reach 28.6 million by 2045. Microfluidic paper-based analytical devices (µPADs) are paper-based analytical tools that use hydrophilic paper for measurement and hydrophobic barriers to control fluid flow. This research aims to develop a non-enzymatic method for detecting glucose and ketones in artificial urine using S2Z-µPADs. The fabrication of S2Z-µPADs involves printing the design on Whatman No. 1 paper using wax printing and applying silver nanoparticles for glucose detection and the Schiff base reaction for ketone detection. The results show that the optimum condition for glucose detection is achieved with an $AgNO_3$ concentration of 500 mM. A NaOH concentration of 10 M. Acetoacetate detection is optimized with a glycine concentration of 1 M, sodium nitroprusside concentration of 15%, NaOH concentration of 1 M, a drying time of 8 minutes, and a reaction time of 10 minutes. Validation results demonstrate good linearity for glucose (R^2 = 0.9821) and ketones (R^2 = 0.995). High precision was achieved with relative standard deviation (RSD) values of 3.792% for glucose and 1.482% for ketones. The obtained limits of detection (LOD) and limits of quantification (LOQ) indicate that the developed S2Z-µPADs can differentiate between each category of diabetes. The accuracy of glucose and ketone detection ranges from 87.463% to 97.374%. The high accuracy of the µPADs highlights their potential for reliable diabetes management and effective disease monitoring.

INTRODUCTION

Diabetes, a chronic disease driven by an unbalanced diet and unhealthy lifestyle, affects millions worldwide. The International Diabetes Federation (IDF) estimates that 537 million adults aged 20-70 will have diabetes in 2021, with projections of 643 million by 2030 and 783 million by 2045. In Indonesia, the prevalence is expected to rise from 19.5 million in 2021 to 28.6 million by 2045, highlighting the need for effective management strategies [1], [2]. Diabetes mellitus, characterized by high blood sugar and disrupted metabolism due to insulin deficiency, leads to fatigue, weight loss, and increased cardiovascular risk. These complications underscore the need for efficient detection methods. Disrupted protein metabolism causes muscle wasting and weakness, further impairing bodily functions. Uncontrolled blood glucose levels can lead to serious complications, emphasizing the

necessity for early detection and more effective detection techniques [3]-[7]. Excess glucose in the blood is filtered by the kidneys and excreted in the urine, a condition known as glycosuria. Diabetes can be diagnosed when the glucose level in the urine reaches 50-100 mg/dL [8], [9]. This condition is often worsened by impaired kidney function [10]. Furthermore, when blood sugar levels in diabetes patients are uncontrolled, the body resorts to fat metabolism for energy, producing ketones. This leads to ketoacidosis, signaling uncontrolled diabetes. Detecting ketones is thus crucial for managing the disease effectively [11], [12]. If there is an excess of ketones, they are transported through the blood to the kidney filtration units and excreted in the urine. The ketones derived from fatty acids by the liver are acetoacetic acid, β-hydroxybutyric acid, and acetone [13], [14].

Glucose levels in urine are useful for the initial screening of advanced diabetes or glycosuria, indicating uncontrolled diabetes [15], [16]. Additionally, ketones can also be used for initial screening in diabetes patients. Their presence in urine, known as ketonuria, indicates ketosis due to carbohydrate deficiency and abnormal glucose metabolism [17]. Hyperglycemia, characterized by persistently high blood sugar levels, is defined by the American Diabetes Association as having blood glucose levels between 100–126 mg/dL (5.6–7 mmol/L), while hyperketonemia occurs when ketone levels in the body are between 6-7.5 mM [18], [19].

Silver nanoparticles (AgNPs) are widely used in glucose detection due to their simple and eco-friendly synthesis. These nanoparticles have various applications, including detection, catalysis, surface modification, and antibacterial action [20], [21]. AgNPs are created directly on cellulose fibers using silver nitrate, which is then reduced to form the nanoparticles. This process is sped up by reducing agents like NaBH4, hydrazine, ethylene glycol [22], or glucose with NaOH [23]. Starch is used to stabilize the nanoparticles, helping to control their size and prevent them from clumping together [24], [25], [26], [27], [28], [29]. Ketone detection in urine for diagnosing diabetes mellitus can be performed using μPADs. This detection method relies on the Schiff base reaction, which forms Schiff bases through the reaction of a primary amine with an aldehyde or ketone carbonyl group. Glycine is used in this reaction for μPADs due to its simplicity, reactivity, and solubility. The Schiff base, containing an imine group, is crucial for creating the magenta complex with sodium nitroprusside [30].

μPADs are paper-based analytical devices first introduced by Whitesides and colleagues in 2007 for detecting proteins and glucose in urine [31], [32], [33]. These devices feature microfluidic patterns and are known for their simplicity, low cost, and ease of use, making them accessible to the general public without requiring specialized skills [34]. Additionally, μPADs are point-of-care testing (POCT) diagnostic devices that comply with the WHO's ASSURED criteria: Affordable, Sensitive, Specific, User-friendly, Rapid and robust, Equipment-free, and Deliverable. A common method used in

glucose detection with µPADs is colorimetry, which involves adding a reagent to the sample, causing a color change that can be analyzed using digital image colorimetry [35]. The colorimetry method has limitations due to ambient light conditions that can affect color intensity. To address these limitations, this study employs a distance-based analysis method.

The present study aims to develop a Distance-Based Single Sample Zone Microfluidic Paper-Based Analytical Device (S2Z-µPADs) for detecting glucose and ketones in the urine. The primary principle involves detecting ketones using sodium nitroprusside, which changes color from brown to purple when reacting with acetoacetic acid, and detecting glucose using silver nitrate, which changes color from clear to brown when reacting with glucose, employing in-situ synthesis for glucose detection.

METHODS
1. Material and Equipment

Whatman No. 1 chromatography paper (GE Healthcare Lifescience, UK), wax/solid ink Xerox ColorQube 850DN, anhydrous D-(+)-glucose (Merck), $AgNO_3$, NaOH were purchased for Emsure, starch (starch-soluble) (Sigma-Aldrich), glycine (≥ 99,7%) (Merck), sodium nitroprusside (99,0%) (Loba Chemie), ethyl acetoacetate, acetone (99,8%) were purchased for Sigma-Aldrich, and distilled water. Additionally, the following materials were used for artificial urine preparation: citric acid monohydrate ($C_6H_8O_7.H_2O$) (Emsure); sodium bicarbonate ($NaHCO_3$) (99,5 – 100,5%), uric acid ($C_5H_4N_4O_3$) (≥ 99%), sodium chloride (NaCl), sodium sulfate decahydrate (Na_2SO_4) (≥ 99,0%), dipotassium hydrogen phosphate (K_2HPO_4) (≥ 99,0%), potassium dihydrogen phosphate (KH_2PO_4) (≥ 99,0%), ammonium chloride (NH_4Cl) (≥ 99,5%), lactic acid ($C_3H_6O_3$) (≥ 98%), calcium chloride dihydrate ($CaCl_2$) (≥ 99,0%), magnesium sulfate heptahydrate ($MgSO_4$) (≥ 99%), and urea (CON_2H_4) were purchased for Sigma-Aldrich.

ColorQube 850DN Solid Ink Color printer was employed to print out S2Z-µPADs. The oven is used to heat the paper, allowing the wax to penetrate the paper's thickness. Software CorelDRAW Graphics Suite X7 was employed to design the S2Z-µPADs. ImageJ was used to measure the slope. Photo box with LED lights provides stable lighting for photographing S2Z-µPADs, mobile camera 12 MP, and glassware.

2. Preparation of S2Z-µPADs

The S2Z-µPADs are fabricated using wax printing. Designed with CorelDRAW Graphics Suite X7, the designs are printed on Whatman No. 1 paper using a Xerox ColorQube 850DN printer, as shown in **Figure 1**. After printing, the paper is heated in an oven at 120°C for 3 minutes to allow the wax to penetrate the paper fully [36]. The paper is then cut according to the design using a paper trimmer or scissors. The back of the S2Z-µPADs is coated with tape. The completed S2Z-µPADs can be stored in a dry cabinet or storage container to maintain humidity.

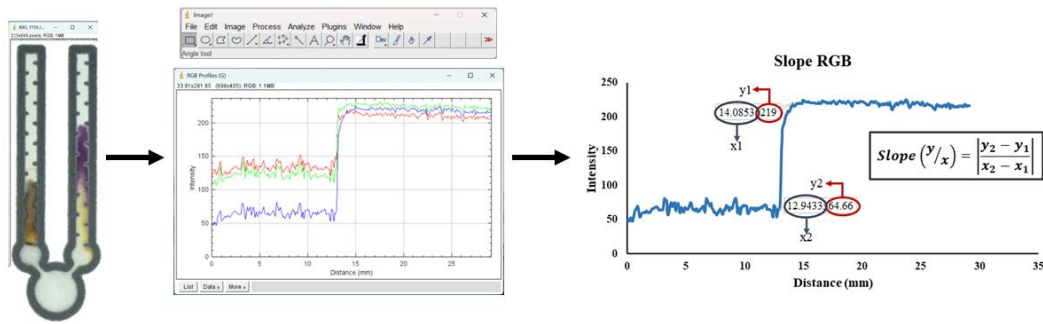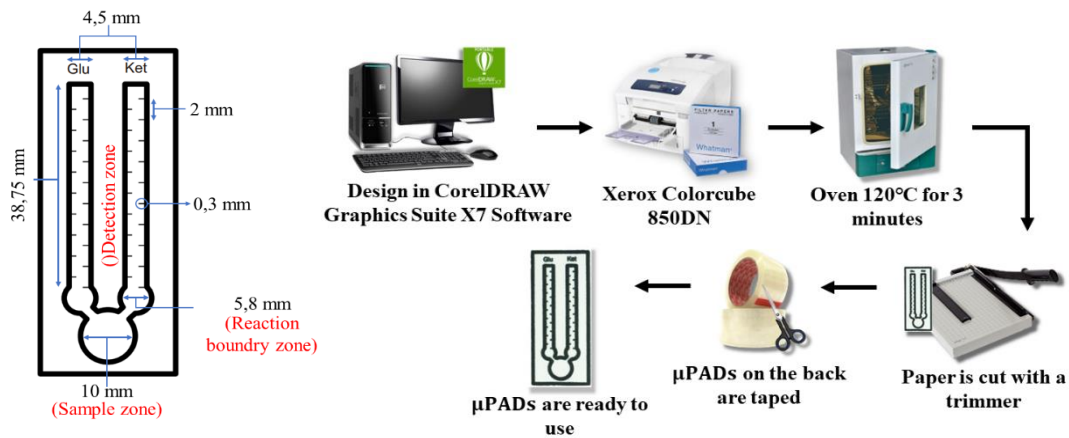**Figure 1.** Design and fabrication of S2Z-µPADs

Figure 2. Slope analysis of S2Z-µPADs using ImageJ

3. Analysis of Glucose and Acetoacetate Detection Distance Reaction

Polymers like pure cellulose fibers are used in the in-situ synthesis of silver nanoparticles (AgNPs) because of their abundance and hydroxyl groups. When reduced to AgNPs, silver nitrate exhibits properties such as catalytic activity, high conductivity, and antibacterial effects. Reducing agents like $NaBH_4$, hydrazine, and ethylene glycol induce a color change during nanoparticle formation. Glucose can also act as a reducing agent with NaOH, accelerating the process and producing smaller particles. Starch is a stabilizer that controls particle size and shape and prevents clumping. In S2Z-µPADs, glucose helps in the in-situ synthesis of AgNPs by reducing silver salts. Glycine, a simple amino acid, is often used for Schiff base formation in µPADs due to its simple structure, reactivity, availability, and water solubility. For ketone detection in urine, the Schiff base contains a carbon-nitrogen double bond called azomethine or imine, which is crucial in the magenta complex reaction with sodium nitroprusside [30].

To prepare the detection zones, an optimal concentration of $AgNO_3$ and a 1% starch solution is applied to the glucose detection zone, spreading from the top of the reaction zone to the bottom. NaOH is then applied at the detection boundary zone. A specific glycine concentration is applied for the ketone detection zone, followed by 15% (w/w) sodium nitroprusside at the detection boundary zone. The device is left to dry for 8

minutes at room temperature. Next, a mixture of 8 mM glucose in artificial urine, 7 mM acetoacetic acid in artificial urine, acetone, and an optimal concentration of NaOH is added to the sample zone and left to dry for 10 minutes.

The analysis is conducted through direct visual observation and using ImageJ software, as illustrated in **Figure 2**. Visual observation monitors the reaction distance and color intensity changes while ImageJ software verifies these observations. The data from ImageJ are presented as RGB graphs. The optimal condition is determined from the slope (y/x) of the RGB graph, where x is the reaction distance and y is the color intensity. The results show the distance of the color change. A higher slope indicates that the change is easily visible, making it possible for the public to analyze the results by directly observing the color change distance. The slope value is expressed in Equation (1).

$$Slope\left(\frac{y}{x}\right) = \left|\frac{y_2 - y_1}{x_2 - x_1}\right|$$

4. Method Validation

Following the determination of optimum conditions, method validation is performed, which includes several tests: measurement of linearity, precision, accuracy, LOD (Limit of Detection), and LOQ (Limit of Quantification). Linearity measurement measures glucose and ketone solutions in artificial urine at 1 to 8 mM concentrations. Precision measurement involves adding glucose and ketone solutions to artificial urine (composition shown in **Table 1**) at concentrations of 8 mM for glucose and 7 mM for ketones, with six repetitions.

Accuracy testing measures glucose and ketones in artificial urine at low, medium, and high levels. LOD and LOQ are determined based on the results of the linearity test. LOD and LOQ are expressed in Equations (2) and (3).

$$LOD = \frac{3,3 \times \sigma}{S} \tag{2}$$

$$LOQ = \frac{10 \times \sigma}{S} \tag{3}$$

Tabel 1. Composition of artifisial urine

Solution Composition	Concentration (mM)
Citric acid	2
Sodium bicarbonate	25
Uric acid	0.4
Sodium chloride	90
Sodium sulfate decahydrate	10
Potassium dihydrogen phosphate	7
Dipotassium hydrogen phosphate	7
Ammonium chloride	25
Lactic acid	1.1
Calcium chloride dihydrate	2.5
Magnesium sulfate	2
Urea	170

RESULTS AND DISCUSSION

1. Heating S2Z-µPADs after Printing

After printing, the S2Z-µPADs are oven-dried at 120°C for 3 minutes to ensure proper wax penetration. Wax viscosity is temperature-dependent, requiring a stable, controlled heat source for consistent results. Wax melts around 120°C. Below this temperature, wax penetration is suboptimal due to incomplete paper absorption. While temperatures above 150°C accelerate wax melting, they also risk damaging the paper substrate. Cellulose fibers in paper are susceptible to damage from high temperatures [37]. **Figure 3** shows a visible difference in the design before and after wax

penetration on both the front and back sides. Before wax penetration, the front design pattern of the S2Z-µPADs exhibits a clear black appearance, while the back design is less distinct or faint. After wax penetration, the front design pattern exhibits wax expansion and color fading, while the back design pattern shows that the wax has penetrated and formed a hydrophobic zone [34], [36]. The design pattern's length and width change after wax penetration is (0.39 x 2.3) mm.
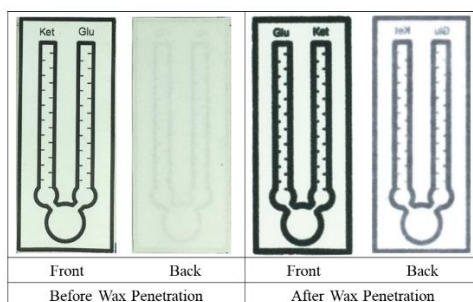

Figure 3. S2Z-µPADs before and after wax penetration (heating)

.

2. The Effect of Reagent and Sample Volume

Optimization of reagent volume is performed on reagent volumes of 7, 8, 9, and 10 µL, as shown in **Figure 4A**. At a reagent volume of 7 µL, the detection zone cannot be fully covered. At 8 µL, the detection zone is fully covered without exceeding its lower limit—9 and 10 µL volumes cause the reagent to spread beyond the detection zone, indicating excess. Therefore, The optimal reagent volume is 8 µL, as it adequately covers the detection zone without causing interference or non-specific color changes, which can affect data accuracy.

Reagent boundary zone volume optimization is conducted with volumes of 0.5, 1, 1.5, and 2 µL, as shown in **Figure 4B**. The optimal volume ensures even spreading across the zone without encroaching into the sample zone. A volume of 0.5 µL does not fully cover the boundary zone, while 1 µL achieves complete coverage without overflow. Volumes of 1.5 and 2 µL cause the reagent to enter the sample zone, affecting migration distance and mixing with the sample. Therefore, the optimal reagent boundary zone volume is 1 µL.

Sample volume optimization is performed with 20, 30, 40, and 50 µL volumes, as shown in **Figure 4C**. Optimization is based on the migration distance within the detection zone. A sample volume of 20 µL results in short migration, underutilizing the detection zone. At 30 µL, migration length is balanced, providing sufficient space for high concentrations of glucose and ketones and allowing measurement of longer migration lengths. Volumes of 40 and 50 µL do not significantly differ in migration length, but 50 µL exceeds the S2Z-µPADs' capacity, causing accumulation in the sample zone and hindering analysis of higher concentrations. Therefore, the optimal sample volume is 30 µL.
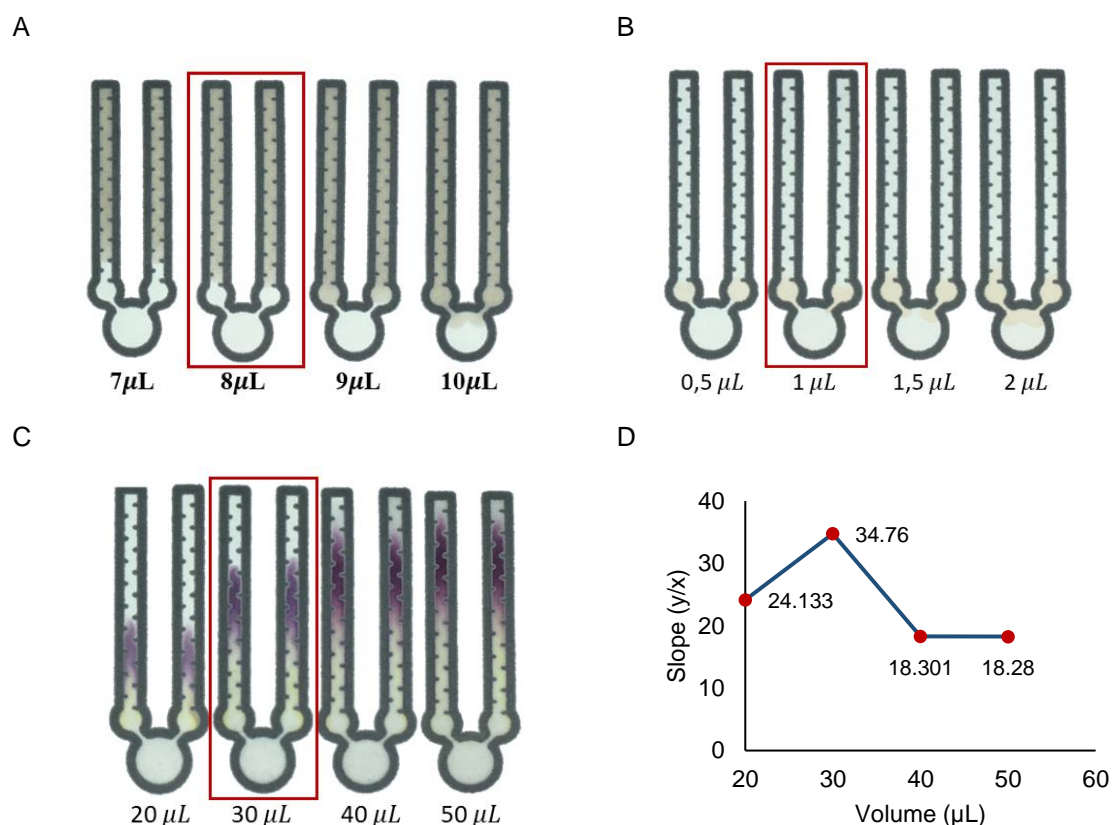
A

7µL   8µL   9µL   10µL

B

0,5 µL   1 µL   1,5 µL   2 µL

C

20 µL   30 µL   40 µL   50 µL

D

Figure 4. Optimization S2Z-µPADs (A) image for reagent volume of glisten, (B) image for reagent volume of sodium nitroprusside Sample volume of ketones, (C) image for a sample volume of ketones (D) The influence of sample volume on the slope intensity of distance reaction.

3. The effect of reagent concentration in the formation of AgNPs

Optimization of AgNO$_3$ concentration is conducted with variations of 100, 500, 1000, 2000, and 3000 mM, as shown in **Figure 5A**. The purpose is to identify the optimal concentration for silver nanoparticle formation in S2Z-µPADs. AgNO$_3$ acts as a precursor ion for Ag$^+$, which is reduced to Ag^0 in the formation of silver nanoparticles [40]. A yellowish-brown color forms at a concentration of 100 mM but is uneven, with a low blue slope value. At 500 mM, the color becomes sharper, resulting in a clearer color change boundary. However, at concentrations above 500 mM, the migration length decreases, and the color darkens,

indicating the reduced ability of 8 mM glucose to reduce AgNO$_3$ due to AgNO$_3$ agglomeration.

Optimization of NaOH concentration is performed with variations of 2, 4, 6, 8, and 10 M, as shown in **Figure 5B**. NaOH acts as a reducing agent for AgNO$_3$ [41]. At 2 M, the color is not visible and is difficult to distinguish with the naked eye. Concentrations from 4 to 10 M produce a visible color change boundary, with the most distinct at 10 M. The brown color produced during glucose detection necessitated the use of a blue color scale for ImageJ analysis [42]. This choice aligns with the complementary color principle and reflects the most significant color change

compared to red and green scales. NaOH concentrations exceeding 10 M exhibit corrosive properties and produce more viscous solutions, making them unsuitable for

small volumes within S2Z-µPADs. Based on the slope value, the optimal NaOH concentration is 10 M.
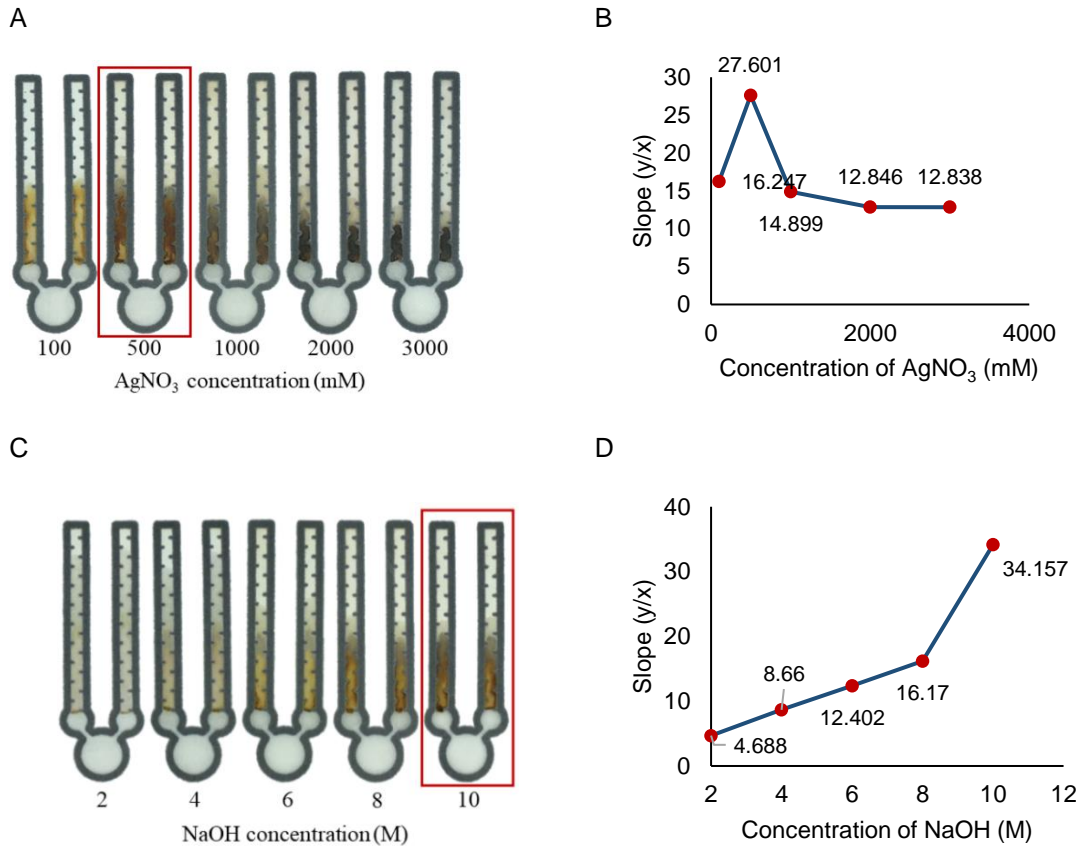
A

B

C

D

Figure 5. Optimization S2Z-µPADs (A) image for the concentration of AgNO₃, (B) the influence of AgNO₃ concentration on the slope intensity of distance reaction, (C) image for the concentration of NaOH, (D) the influence of NaOH concentration on the slope intensity of distance reaction.

4. The Effect of Reagent Concentration in the Formation of Magenta Complexes

Figure 6A presents the optimization of glycine concentration, performed with variations of 0.1, 0.5, 1, 1.5, and 2 M. Glycine is crucial in forming imine derivatives [43]. Higher glycine concentrations lead to more magenta complex formation. The effect of glycine concentration is analyzed using ImageJ software by observing the green slope. The sample used is ketone in artificial urine at a concentration of 7 mM. Based on ImageJ analysis, the optimal slope value occurs at a glycine concentration of 1 M. Insufficient glycine can react with all the carbonyl compounds at low glycine concentrations, resulting in a less pronounced color change. However, at higher glycine concentrations, an adverse effect emerges. Excess glycine can act as a binding agent, sequestering carbonyl compounds and rendering them unavailable

for the condensation reaction. Therefore, the optimal glycine concentration is 1 M.
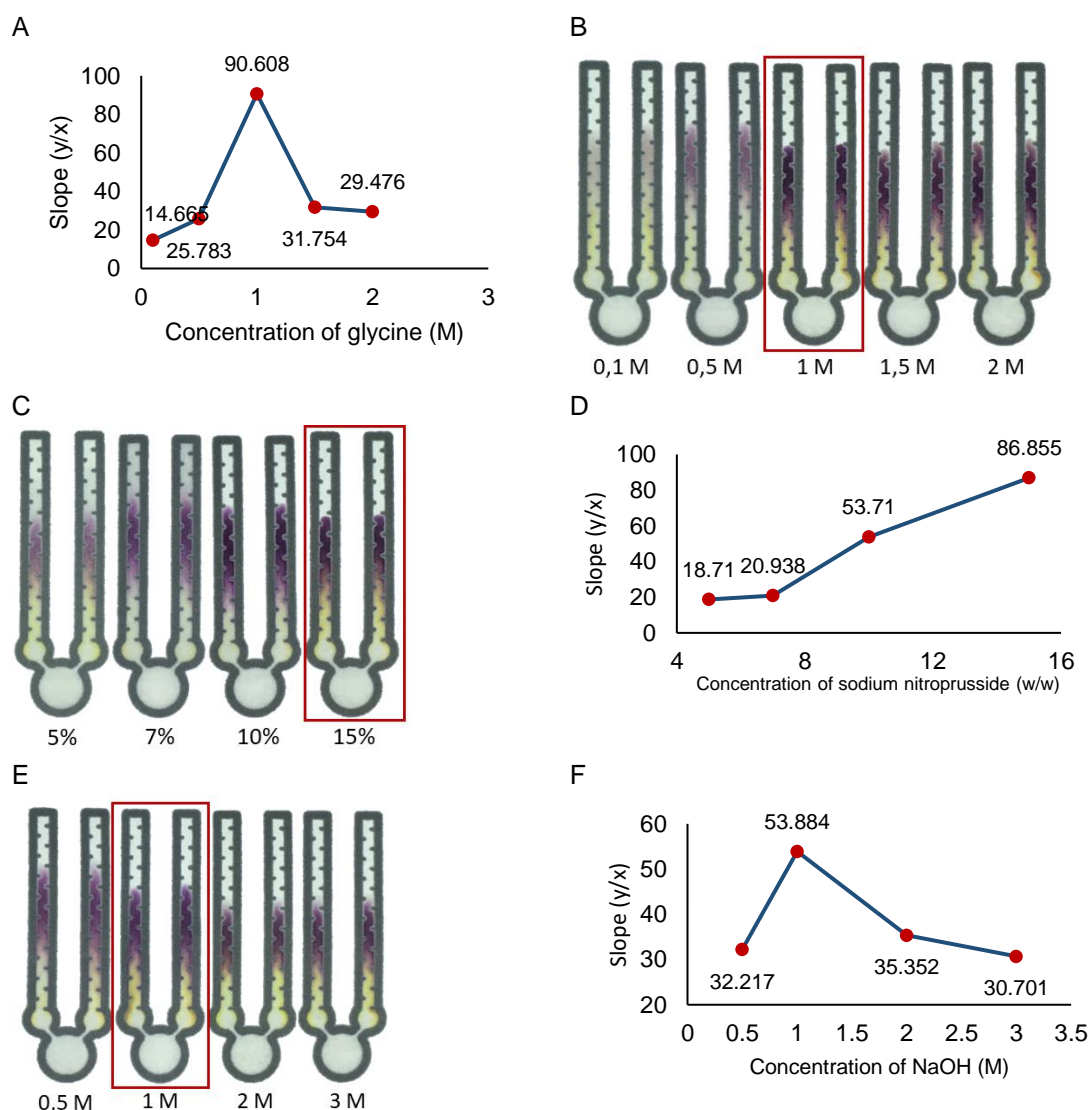
A

B

C

D

E

F

Figure 6. Optimization S2Z-µPADs (A) image for concentration of glycine, (B) the influence of glycine concentration on the slope intensity of distance reaction, (C) image for concentration of sodium nitrusside, (D) the influence of sodium nitrusside concentration on the slope intensity of distance reaction, (E) image for concentration of NaOH, (F) the influence of NaOH concentration on the slope intensity of distance reaction

Figure 6C presents the optimization of sodium nitrusside concentration, performed with variations of 5%, 7%, 10%, and 15% (w/w). Sodium nitrusside is involved in the formation of the magenta complex [44]. Higher concentrations lead to more imine derivatives formation. The sample used is ketone in artificial urine at a concentration of 7 mM. Based on ImageJ analysis, the green slope value increases at a concentration of 15% (w/w), where solubility becomes difficult to achieve.

Figure 6E presents the optimization of NaOH concentration in the sample zone, performed with variations of 0.5, 1, 2, and 3 M with a mixture of 7 mM ketone solution in

artificial urine. NaOH provides the basic environment needed for glycine deprotonation [38]. Based on ImageJ analysis, the green slope value increases at a concentration of 1 M. The color change boundary is most distinct and clear at this concentration. Therefore, the optimal NaOH concentration is 1 M. At low NaOH concentrations (0.5 M), insufficient catalyst hinders the reaction's progress, resulting in a faint color change boundary and a low slope value. A concentration of 1 M NaOH strikes an optimal balance between catalyst and reagents, enabling efficient condensation and maximizing Schiff base formation. However, the catalytic effect becomes excessive at higher NaOH concentrations (2-3 M). Excess NaOH can significantly increase the solution's pH, disrupting the condensation reaction equilibrium and impeding Schiff base formation.

Drying time optimization is performed with variations of 0, 5, 8, and 10 minutes, as shown in **Figure 7**. Optimizing reagent drying time is crucial for maintaining reagent mobility and ensuring consistent detection across the S2Z-µPADs. Faster drying times result in a more faded color change boundary, making it difficult to observe with the naked eye. Inadequate drying time (0-5 minutes) hinders reagent diffusion, leading to uneven distribution and a faint color change. The optimal drying time of 8 minutes allows for sufficient diffusion, resulting in a well-defined color change boundary and a high slope value. However, excessive drying (10 minutes) causes over-drying, reducing reagent mobility and leading to uneven detection zones and inconsistent color, particularly in the glucose detection zone— the fainter color change boundary results in a lower slope value. Therefore, the optimal drying time is 8 minutes.

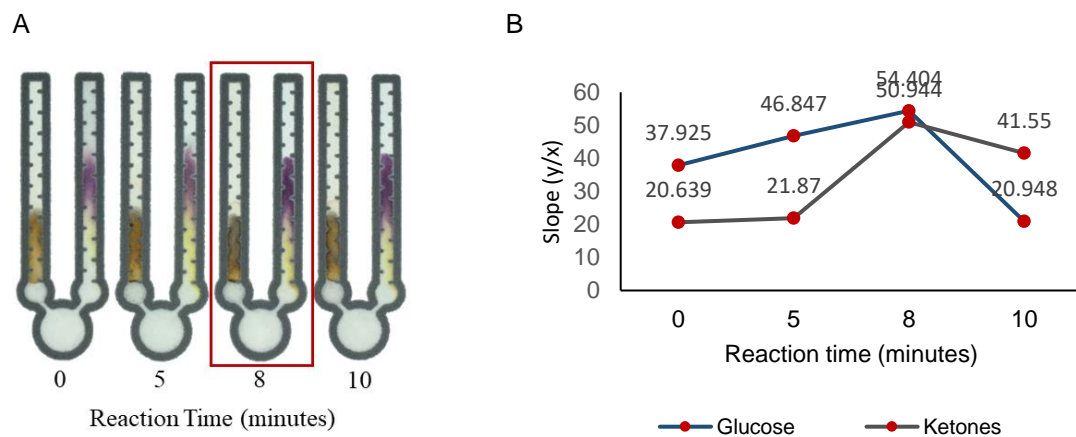## 5. The Effect of Reagent Drying Time

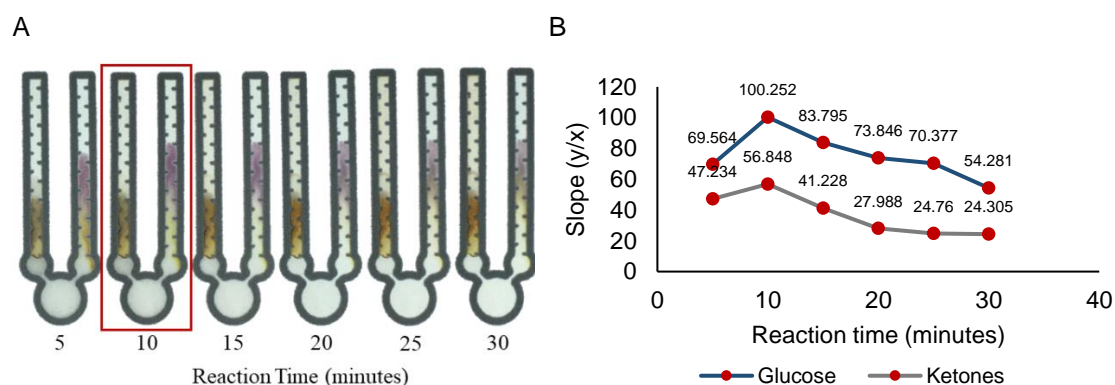**Figure 7.** Optimization S2Z-µPADs (A) image for drying time, (B) the influence of drying time on the slope intensity of distance reaction

6. The Effect of Reaction Time

Reaction time optimization is performed with variations of 5, 10, 15, 20, 25, and 30 minutes, as shown in **Figure 8**. Reaction time affects the formation of AgNPs in glucose detection and the magenta

complex in ketone detection. At a reaction time of 5 minutes, the reaction process is incomplete, leading to a change in migration length of 10 minutes. For reaction times exceeding 10 minutes, the color change boundary remains consistent. ImageJ analysis indicates that glucose and ketone

.

detection's optimal color intensity slope value occurs at 10 minutes. Although longer reaction times typically produce more products, extended exposure to oxygen beyond 10 minutes can cause product decomposition [45], resulting in decreased color intensity.

A   B

Figure 8. Optimization S2Z-µPADs (A) image for reaction time, (B) the influence of reaction time on the slope intensity of distance reaction.

7. Method validation

Following optimization, method validation is conducted using the optimal concentrations. **Figure 9A** displays the results of linearity testing, where glucose and acetoacetate solutions in artificial urine (ranging from 1-8 mM) are measured. A strong linear relationship is achieved for glucose detection with a coefficient of determination ($R^2 = 0.9821$). Similarly, ketone detection shows a high coefficient of determination ($R^2 = 0.995$). This strong linearity is vital for accurate quantification, ensuring that color intensity changes directly reflect analyte concentration changes. This enables reliable conversion of color change distance into actual concentrations of glucose or ketones in the sample.

Figure 9B shows the precision testing results, indicating consistent measurements for glucose and ketone solutions in artificial urine. The relative standard deviation (RSD) for glucose measurement is 3.792%, and for ketone measurement, it is 1.482%, demonstrating good precision.

Figure 9C highlights the accuracy testing performed at low, medium, and high levels of glucose and ketones in artificial urine. The accuracy results range from 87.463% to 97.374%, indicating that the S2Z-µPADs provide reliable measurements. High accuracy is essential for real-world applications, making S2Z-µPADs a potentially portable and user-friendly alternative to existing methods.

The Limit of Detection (LOD) and Limit of Quantification (LOQ) for glucose detection are 0.98 mM and 2.99 mM, respectively. The LOD is 1.78 mM for ketone detection, and the LOQ is 5.41 mM. According to Mukhopadhyay (2022), glucose levels can be categorized as normal (≤2 mM), moderate (2-5 mM), high (5-9 mM), and very high (9-13 mM). Ketone levels are categorized as normal (≤2 mM), moderate (2-4 mM), high (4-8 mM), and very high (>8 mM) [39].
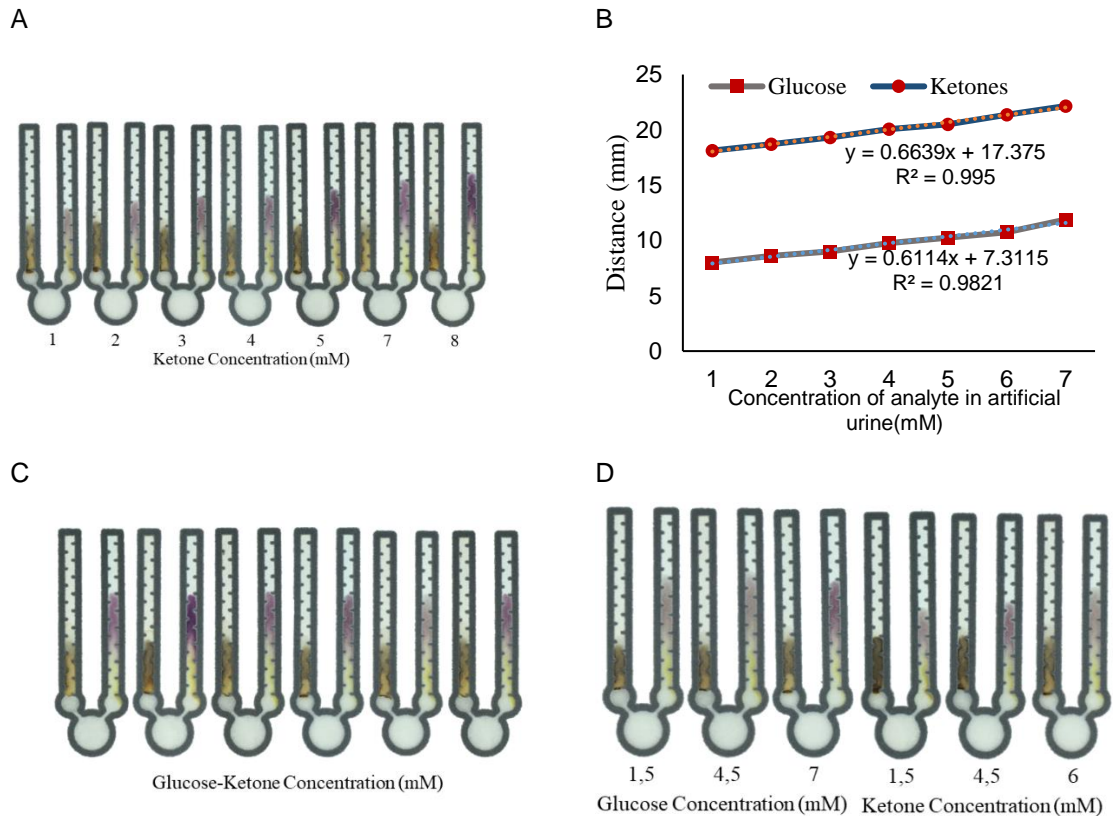
A

B

C

D

Figure 9. S2Z-µPADs (A) image for linearity, (B) the influence of linearity on the slope intensity of distance reaction, (C) image for precision, (D) image for accuracy

CONCLUSION

A novel method for non-enzymatic detection of glycosuria and ketonuria has been successfully developed using paper-based substrates. This innovative approach uses silver nitrate for synthesizing silver nanoparticles (AgNPs) to detect glucose and employs Schiff base synthesis and a sodium nitroprusside test for ketone detection. The method uses a distance-based design with a single sample zone (S2Z-µPADs), eliminating the need for additional instruments by relying on the analysis of color migration length changes. This makes the analytical tool inexpensive, portable, and easy to use. The research optimized conditions for the S2Z-µPADs method: 500 mM $AgNO_3$ and 10 M NaOH proved optimal for glucose detection. The best results were obtained with 1 M glycine, 15% sodium nitroprusside (w/w), and 1 M NaOH for detecting acetoacetate. The reagent volume

in the detection zone was set at 8 µL, the detection limit zone reagent volume at 1 µL, and the sample volume at 30 µL. The optimal drying time was 8 minutes, with a reaction time of 10 minutes. Method validation showed excellent performance. For glucose detection, the results demonstrated strong linearity (R^2 = 0.9821), good precision (RSD of 3.792%), accuracy ranging from 89.27% to 93.43%, an LOD of 0.98 mM, and an LOQ of 2.99 mM. For ketone detection, the method achieved a high coefficient of determination (R^2 = 0.995), precision with an RSD of 1.482%, accuracy between 87.46% and 97.37%, an LOD of 1.78 mM, and an LOQ of 5.41 mM.This approach offers a promising, user-friendly alternative for diabetes monitoring, ensuring reliable and accurate urine detection of glucose and ketones.

ACKNOWLEDGEMENT

REFERENCES

[1] E. Mozzillo, F. Zanfardino, C. Madeo, A. Rossi, R. Spadaro, G. Monzani, M. Santoro, F. Rollato, L. Iafusco, and L. Tinto, "Unhealthy lifestyle habits and diabetes-specific health-related quality of life in youths with type 1 diabetes," *Acta Diabetol.*, vol. 54, no. 12, pp. 1073–1080, Dec. 2017, doi: 10.1007/s00592-017-1051-5.

[2] D. Atlas, *International Diabetes Federation*, 2nd ed. Brussels, Belgium: International Diabetes Federation, 2015.

[3] American Diabetes Association, "Diagnosis and Classification of Diabetes Mellitus," *Diabetes Care*, vol. 37, no. Supplement_1, pp. S81–S90, Jan. 2014.

[4] U. Alam, C. R. Asghar, R. F. Frost, S. Kumar, and J. Malik, "General aspects of diabetes mellitus," in *Handbook of Clinical Neurology*, vol. 126, Elsevier, 2014, pp. 211–222, doi:10.1016/B978-0-444-53480-4.00016-3.

[5] S. Todkar, "Diabetes Mellitus the 'Silent Killer' of mankind: An overview on the eve of World Health Day!," *J. Med. Allied Sci.*, vol. 6, no. 1, p. 39, 2016, doi: 10.5455/jmas.214333.

[6] V. Kumar and K. D. Gill, "Qualitative Analysis of Ketone Bodies in Urine," in *Basic Concepts in Clinical Biochemistry: A Practical Guide*, Singapore: Springer Singapore, 2018, pp. 119–122, doi: 10.1007/978-981-10-8188-8_29.

[7] K. Kaul, B. N. Tarr, P. K. Sharma, and D. K. Dutt, "Introduction to Diabetes Mellitus," *Diabetes Old Dis.*, 2013, doi: 10.1007/978-3-642-17458-0_1.

[8] S. Prapaporn, T. Woranart, and P. Phisit, "Nanocellulose Films to Improve the Performance of Distance-based Glucose Detection in Paper-based Microfluidic Devices," *Anal. Sci.*, vol. 36, no. 12, pp. 1447–1451, Dec. 2020, doi: 10.2116/analsci.20P207.

[9] J. C. G. Coolen and J. Verhaeghe, "Physiology and clinical value of glycosuria after a glucose challenge during pregnancy," *Eur. J. Obstet. Gynecol. Reprod. Biol.*, vol. 150, no. 2, pp. 132–136, Jun. 2010, doi: 10.1016/j.ejogrb.2010.02.003.

[10] M. R. Clarkson, M. D. Magee, C. E. Pickering, and B. R. Gilbert, "Chapter 2 - Laboratory Assessment of Kidney Disease," in *Pocket Companion to*

Brenner and Rector's The Kidney (Eighth Edition), Philadelphia: W.B. Saunders, 2011, pp. 21–41, doi: 10.1016/B978-1-4160-6195-1.00002-3.

[11] J. Huang, X. Liang, J. Lin, and C. Zhang, "Update on Measuring Ketones," *J. Diabetes Sci. Technol.*, vol. 18, no. 3, pp. 714–726, May 2024, doi: 10.1177/19322968231168314.

[12] S. Misra and N. S. Oliver, "Utility of ketone measurement in the prevention, diagnosis and management of diabetic ketoacidosis," *Diabet. Med.*, vol. 32, no. 1, pp. 14–23, Jan. 2015, doi: 10.1111/dme.12604.

[13] S. Mitra, M. K. Pal, S. Roy, and P. Sengupta, "Digital electronic based portable device for colorimetric quantification of ketones and glucose level in human urine," *Measurement*, vol. 214, p. 112848, Jun. 2023, doi:10.1016/j.measurement.2023.112848

[14] B. J. Stubbs, E. Cox, C. Evans, and D. Clarke, "On the Metabolism of Exogenous Ketones in Humans," *Front. Physiol.*, vol. 8, p. 848, Oct. 2017, doi: 10.3389/fphys.2017.00848.

[15] M.-Y. Jia, T. A. Nguyen, C. Jin, and Y. Wang, "The calibration of cellphone camera-based colorimetric sensor array and its application in the determination of glucose in urine," *Biosens. Bioelectron.*, vol. 74, pp. 1029–1037, Dec. 2015, doi: 10.1016/j.bios.2015.06.034.

[16] A. Brown, L. R. Chalmers, and P. Mancini, "Insulin-associated weight gain in obese type 2 diabetes mellitus patients: What can be done?," *Diabetes Obes. Metab.*, vol. 19, no. 12, pp. 1655–1668, Dec. 2017, doi: 10.1111/dom.13007.

[17] C. Chairani and S. Karlina, "Pemeriksaan Keton Urine Pada Pasien Diabetes Melitus," *Pros. Semin.*

Kesehat. Perintis, vol. 3, no. 1, pp. 150–154, 2020.

[18] B. Giri, "Chronic hyperglycemia mediated physiological alteration and metabolic distortion leads to organ dysfunction, infection, cancer progression and other pathophysiological consequences: An update on glucose toxicity," *Biomed. Pharmacother.*, vol. 107, pp. 306–328, 2018, doi: 10.1016/j.biopha.2018.07.154.

[19] V. Kumar, A. K. Singh, R. Tripathi, and A. Kumar, "Ketoalkalosis: Masked Presentation of Diabetic Ketoacidosis With Literature Review," *J. Endocrinol. Metab.*, vol. 7, no. 6, pp. 194–196, 2017, doi: 10.14740/jem400w.

[20] B.-H. Jun, "Silver Nano/Microparticles: Modification and Applications," *Int. J. Mol. Sci.*, vol. 20, no. 11, p. 2609, May 2019, doi: 10.3390/ijms20112609.

[21] E. Susilowati, P. Purnamasari, and S. M. Widiastuti, "Preparation of Silver-Chitosan Nanocomposites Colloidal and Film as Antibacteri Material," *JKPK J. Kim. Dan Pendidik. Kim.*, vol. 5, no. 3, p. 300, Dec. 2020, doi: 10.20961/jkpk.v5i3.46711.

[22] G. Chen, Y. Hu, and C. Sun, "In Situ Synthesis of Silver Nanoparticles on Cellulose Fibers Using D-Glucuronic Acid and Its Antibacterial Application," *Materials*, vol. 12, no. 19, p. 3101, Sep. 2019, doi: 10.3390/ma12193101.

[23] K.-S. Chou and Y.-S. Lai, "Effect of polyvinyl pyrrolidone molecular weights on the formation of nanosized silver colloids," *Mater. Chem. Phys.*, vol. 83, no. 1, pp. 82–88, Jan. 2004, doi: 10.1016/j.matchemphys.2003.09.031.

[24] H. S. Budi, D. H. Pratama, and M. I. T. Khair, "Synthesis of Polystyrene Fiber Membranes Prepared by Electrospinning: Effect of AgNO3 on the Microstructure," *JKPK J. Kim. Dan Pendidik. Kim.*, vol. 9, no. 1, p. 130, Apr. 2024,
doi: 10.20961/jkpk.v9i1.84601.

[25] T. Pinheiro, P. Pinto, C. Maia, and A. S. Almeida, "Paper-Based In-Situ Gold Nanoparticle Synthesis for Colorimetric, Non-Enzymatic Glucose Level Determination," *Nanomaterials*, vol. 10, no. 10, p. 2027, Oct. 2020, doi: 10.3390/nano10102027.

[26] E. Susilowati, S. Oktaviani, and A. Handayani, "Synthesin and Characterization Chitosan Film with Silver Nanoparticle Addition As A Multiresistant Antibacteria Material," *JKPK J. Kim. Dan Pendidik. Kim.*, vol. 6, no. 3, p. 371, Dec. 2021, doi: 10.20961/jkpk.v6i3.57101.

[27] X. Gao, Z. Dai, and Z. Shi, "Green synthesis and characteristic of core-shell structure silver/starch nanoparticles," *Mater. Lett.*, vol. 65, no. 19–20, pp. 2963–2965, Oct. 2011, doi: 10.1016/j.matlet.2011.06.065.

[28] V. Raji, S. Anirudhan, and J. Paul, "Synthesis of Starch-Stabilized Silver Nanoparticles and Their Antimicrobial Activity," *Part. Sci. Technol.*, vol. 30, no. 6, pp. 565–577, Nov. 2012, doi: 10.1080/02726351.2012.701789.

[29] Y. Pratiwi, R. Kusuma, and A. B. Lestari, "Biosynthesis of Poly Acrylic Acid (PAA) Modified Silver Nanoparticles, Using Basil Leaf Extract (Ocimum basilicum L.) for Heavy Metal Detection," *JKPK J. Kim. Dan Pendidik. Kim.*, vol. 8, no. 3, p. 323, Dec. 2023, doi: 10.20961/jkpk.v8i3.78641.

[30] F. M. Ibrahim and S. M. Abdalhadi, "Performance of Schiff Bases Metal Complexes and their Ligand in Biological Activity: A Review," *Al-Nahrain J. Sci.*, vol. 24, no. 1, pp. 1–10, Mar. 2021,
doi: 10.22401/ANJS.24.1.01.

[31] T. Kaneta, Y. Karita, and K. Kaneko, "Microfluidic paper-based analytical devices with instrument-free detection and miniaturized portable detectors," *Appl. Spectrosc. Rev.*, vol. 54, no. 2, pp. 117–141, Feb. 2019, doi: 10.1080/05704928.2018.1465505.

[32] E. Noviana, R. J. McCord, M. G. Clark, and S. R. Henry, "Microfluidic Paper-Based Analytical Devices: From Design to Applications," *Chem. Rev.*, vol. 121, no. 19, pp. 11835–11885, Oct. 2021, doi: 10.1021/acs.chemrev.1c00160.

[33] L.-M. Fu and Y.-N. Wang, "Detection methods and applications of microfluidic paper-based analytical devices," *TrAC Trends Anal. Chem.*, vol. 107, pp. 196–211, Oct. 2018, doi: 10.1016/j.trac.2018.08.006.

[34] D. M. Cate, J. A. Adkins, J. Mettakoonpitak, and C. S. Henry, "Simple, distance-based measurement for paper analytical devices," *Lab. Chip*, vol. 13, no. 12, p. 2397, 2013, doi: 10.1039/c3lc00096k.

[35] M. Rahbar, J. Bruch, and D. M. Cate, "Ion-Exchange Based Immobilization of Chromogenic Reagents on Microfluidic Paper Analytical Devices," *Anal. Chem.*, vol. 91, no. 14, pp. 8756–8761, Jul. 2019,
doi: 10.1021/acs.analchem.9b00848.

[36] M. I. Sari, R. D. Ningrum, and E. E. Siswanta, "Microfluidic Paper based Analytical Device (μpads) for Analysis of Benzoat Acid in Packaged Beverages," *IOP Conf. Ser. Mater. Sci. Eng.*, vol. 546, no. 3, p. 032028, Jun. 2019, doi: 10.1088/1757-899X/546/3/032028.

[37] Y. F. Wisang, A. H. Pramudya, and A. R. Maharani, "Microfluidic Paper-based Analytical Devices (μPADs) For Analysis Lead Using Naked Eye and Colorimetric Detections," *IOP Conf. Ser. Mater. Sci. Eng.*, vol. 546, no. 3, p. 032033, Jun. 2019,
doi: 10.1088/1757-899X/546/3/032033.

[38] K. Bakalorz, K. Rybarczyk, and L. Biernat, "Unprecedented Water Effect as a Key Element in Salicyl-Glycine Schiff Base Synthesis," *Molecules*, vol. 25, no. 5, p. 1257, Mar. 2020, doi: 10.3390/molecules25051257.

[39] M. Mukhopadhyay, A. Goswami, and P. Mondal, "Laser printing based colorimetric paper sensors for glucose and ketone detection: Design, fabrication, and theoretical analysis," *Sens. Actuators B Chem.*, vol. 371, p. 132599, Nov. 2022, doi: 10.1016/j.snb.2022.132599.

[40] H. I. Salaheldin, "Optimizing the synthesis conditions of silver nanoparticles using corn starch and their catalytic reduction of 4-nitrophenol," *Adv. Nat. Sci. Nanosci. Nanotechnol.*, vol. 9, no. 2, p. 025013, Jun. 2018, doi: 10.1088/2043-6254/aac4eb.

[41] G. Eka Putri, F. Rahayu Gusti, A. Novita Sary, and R. Zainul, "Synthesis of silver nanoparticles used chemical reduction method by glucose as reducing agent," *J. Phys. Conf. Ser.*, vol. 1317, no. 1, p. 012027, Oct. 2019, doi: 10.1088/1742-6596/1317/1/012027.

[42] M. Singh, I. Sinha, and R. K. Mandal, "Role of pH in the green synthesis of silver nanoparticles," *Mater. Lett.*, vol. 63, no. 3–4, pp. 425–427, Feb. 2009, doi:10.1016/j.matlet.2008.10.067.

[43] U. Sani, H. U. Na'ibi, and S. A. Dailami, "In vitro antimicrobial and antioxidant studies on N-(2- hydroxylbenzylidene) pyridine -2-amine and its M(II) complexes," *Niger. J. Basic Appl. Sci.*, vol. 25, no. 1, p. 81, Jul. 2018, doi: 10.4314/njbas.v25i1.11.

[44] S. A. Klasner, A. K. Price, K. W. Hoeman, R. S. Wilson, K. J. Bell, and C. T. Culbertson, "Paper-based microfluidic devices for analysis of clinically relevant analytes present in urine and saliva," *Anal. Bioanal. Chem.*, vol. 397, no. 5, pp. 1821–1829, Jul. 2010, doi: 10.1007/s00216-010-3718-4.

[45] T. Hüppe, D. Lorenz, F. Maurer, T. Fink, R. Klumpp, and S. Kreuer, "Quantification of Volatile Acetone Oligomers Using Ion-Mobility Spectrometry," *J. Anal. Methods Chem.*, vol. 2021, pp. 1–6, Aug. 2021, doi: 10.1155/2021/6638036.